21 Mori K, Suzuki T, Uozaki H *et al.* Detection of minimal gastric cancer cells in peritoneal washings by focused microarray analysis with multiple markers: clinical implications. *Ann Surg Oncol* 2007; **14**: 1694–702.
22 Markman M, Brady MF, Spirtos NM, Hanjani P, Rubin SC. Phase II trial of intraperitoneal paclitaxel in carcinoma of the ovary, tube, and peritoneum: a gynecologic oncology group study. *J Clin Oncol* 1998; **16**: 2620–4.
23 Nishiyama M, Wada S. Docetaxel: its role in current and future treatments for advanced gastric cancer. *Gastric Cancer* 2009; **12**: 132–41.
24 Haren L, Remy MH, Bazin I, Callebaut I, Wright M, Merdes A. NEDD1-dependent recruitment of the gamma-tubulin ring complex to the centrosome is necessary for centriole duplication and spindle assembly. *J Cell Biol* 2006; **172**: 505–15.
25 Inoue M, Matsumoto S, Saito H, Tsujitani S, Ikeguchi M. Intraperitoneal administration of a small interfering RNA targeting nuclear factor-kappa B with paclitaxel successfully prolongs the survival of xenograft model mice with peritoneal metastasis of gastric cancer. *Int J Cancer* 2008; **123**: 2696–701.
26 Takeshita F, Patrawala L, Osaki M *et al.* Systemic delivery of synthetic microRNA-16 inhibits the growth of metastatic prostate tumors via downregulation of multiple cell-cycle genes. *Mol Ther* 2010; **18**: 181–7.
27 Ueda T, Volinia S, Okumura H *et al.* Relation between microRNA expression and progression and prognosis of gastric cancer: a microRNA expression analysis. *Lancet Oncol* 2010; **11**: 136–46.
28 Yanagihara K, Tsumuraya M. Transforming growth factor β1 induces apoptotic cell death in cultured human gastric carcinoma cells. *Cancer Res* 1992; **52**: 4042–5.
29 Saeki N, Kim DH, Usui T *et al.* GASDERMIN, suppressed frequently in gastric cancer, is a target of LMO1 in TGF-β-dependent apoptotic signalling. *Oncogene* 2007; **26**: 6488–98.

doi: 10.1111/cas.12054

Chapter 17

In Vivo Imaging of Oligonucleotide Delivery

Fumitaka Takeshita, Ryou-u Takahashi, Jun Onodera, and Takahiro Ochiya

Abstract

RNA interference (RNAi) has rapidly become a powerful tool for drug-target discovery and therapeutics. Cancer is an important application for RNAi therapeutics, since abnormal gene regulation is thought to contribute to the pathogenesis and maintenance of the metastatic phenotype of cancer. Many oncogenic genes present enticing therapeutic target possibilities for RNAi. Small interfering RNA (siRNA) and microRNA (miRNA) are potent and specific examples of RNAi are able to silence tumor-related genes and multiple oncogenic pathways and appear to be a rational approach to inhibit tumor growth. In subsequent in vivo studies, an appropriate animal model must be developed for a better evaluation of gene-silencing effects on tumors. How to evaluate the effect of siRNA and miRNA in an in vivo therapeutic model is also important. Bioluminescence imaging is an optical imaging method that can evaluate RNAi in vivo.

Key words: siRNA, MicroRNA, Cancer, Delivery, Imaging, Luciferase, Oligonucleotides

1. Introduction

RNAi can effect posttranscriptional gene silencing. The introduction into an organism of double-stranded RNA (dsRNA) corresponding to a transcribed sequence results in degradation of the corresponding mRNA (1–6). With RNAi, dsRNA blocks gene expression in a sequence-specific manner. When introduced into cells, dsRNA is processed by the RNase III family nuclease Dicer into siRNA, 21-basepair dsRNA with two overhanging bases at each 3′ terminus. The double-stranded siRNA is passed to the RNA-induced silencing complex (RISC), an RNA–nuclease complex, which is activated as it unwinds the duplex and incorporates one of the antisense strands. The RISC then selectively degrades

Robert M. Hoffman (ed.), *In Vivo Cellular Imaging Using Fluorescent Proteins: Methods and Protocols*,
Methods in Molecular Biology, vol. 872, DOI 10.1007/978-1-61779-797-2_17,

RNA containing the sequence complementary to the incorporated antisense strand.

Antisense oligonucleotide drugs were used prior to the discovery of RNAi and several antisense molecules are currently in late-stage preclinical or clinical development (7). Although researchers continue to explore and develop antisense reagents for therapeutic use by morpholino oligomers, a fourth class of oligonucleotide-based compounds, consisting of siRNAs, has recently become widely used for gene knockdown in vitro and in vivo.

Another group of catalytically-active RNA molecules (ribozymes) has also been considered for therapeutic use. However, only a few ribozymes have turned out to be efficient compounds in clinical trials. RNAi is effective because siRNA is highly specific for the target gene, and the single-strand RNA molecule incorporated into the RISC is used to recognize multiple copies of the target RNA. Therefore, an extremely small amount of siRNA can generate reliable gene suppression, making toxicity less of a concern. Furthermore, effective antisense oligonucleotide sequences are determined empirically, resulting in uncertain efficacies.

MicroRNA (miRNA), an endogenously-expressed form of siRNA, approximately 22 nucleotides in length, also works for gene silencing. It is estimated that there are over 1,000 miRNAs in humans. It is believed that a single miRNA can regulate several hundred genes. Current understanding of the molecular mechanism of any disease, including cancer (8, 9), would be incomplete without factoring in the functional significance of miRNA. Misexpression of miRNAs has been observed in various types of cancers and is also associated with the clinical outcome of cancer patients. Consistently, miRNAs have been implicated in the regulation of various cellular processes that are often deregulated during tumor development and progression (10, 11), suggesting that these miRNAs might be targets for cancer therapy.

The most direct way for molecules to correct expression of altered genes and miRNAs is treatment by RNA oligonucleotides. For this purpose, an in vivo delivery system is a key issue. Here, we describe an in vivo imaging method of delivery of oligonucleotides such as siRNA and miRNA.

2. Materials

2.1. Cell Lines and Medium

1. PC-3M-luc cells (Xenogen Corp., Alameda, CA).
2. Cell culture medium: RPMI 1640 medium (Invitrogen Corp., Carlsbad, CA) supplemented with 10% heat-inactivated fetal bovine serum (Equitech-Bio, Kerrville, TX) and 0.2 mg/ml zeocin (Invitrogen Corp.).

2.2. Oligonucleotide Delivery Mixture

1. Oligonucleotide delivery system: atelocollagen (12–15) for local use AteloGene™ #1390 and systemic use AteloGene™ #1391 (Koken, Tokyo).
2. Oligonucleotides: 5–10 and 20–40 μM oligonucleotide solutions for local and systemic delivery in vivo.

2.3. In Vivo Imaging

1. For in vivo imaging with Renilla luciferase: ViviRen (5 mg/kg, Promega).
2. For in vivo imaging with firefly luciferase: D-luciferin (150 mg/kg, Xenogen).
3. Data analysis: LivingImage software (version 2.50, Xenogen) (16).

3. Methods

Recent progress in the optical imaging of cancers in animal models presents many potential advantages for recreating the disease process, disease detection, screening, diagnosis, drug development, and treatment evaluation. Fluorescence-based imaging (17–21) and bioluminescence-based imaging (12, 13, 22–29) are well developed and allow specific, highly-sensitive, and quantitative measurements of a wide range of tumor-related parameters in mice.

A major advantage of GFP-labeling is that imaging requires no preparative procedures and hence allows for direct visualization in living tissue. In contrast, luciferase imaging requires exogenous injection of luciferin substrate which can stress the animals. In addition, the intensity of the luciferase signal may sometimes be variable and unstable. Furthermore, RFP imaging is about 1,000 times stronger than that of luciferase in vivo. Therefore, for monitoring the tumor metastasis process at the single-cell level, fluorescence imaging may be the more practical method. In fact, fluorescence-based orthotopic metastatic models have been used to study mechanisms and drug discovery. Here, we have used the bioluminescence signal from the luciferase reporter gene in our metastasis model. Luciferase genes in our tumor cells can function stably over significant periods of time in tumors and in their metastases.

3.1. Preparation of Dual Luciferase Expressing Cells

1. For construction of 3′-UTR-Renilla luciferase plasmid and reporter assays, amplify the segment of 3′-UTR of the Bcl2 gene by PCR using genomic DNA from normal human prostate epithelial cells (PrEC, CT-2555, Lonza Walkersville, Inc., Walkersville, MD).
2. Insert the PCR product into a pGL4.75 [HRuc/CMV] vector (Promega, Madison, WI), using the XbaI site immediately

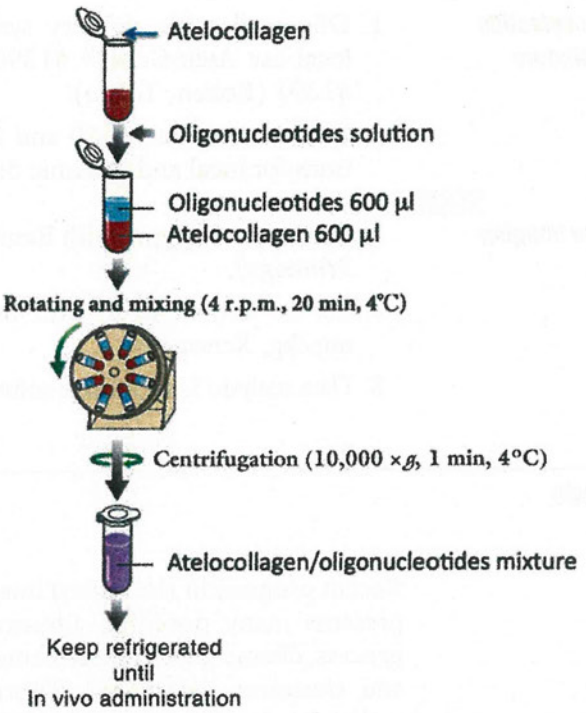

Fig. 1. Preparation of oligonucleotides delivery mixture. Gently add 600 µl of the oligonucleotide solution to 600 µl of the atelocollagen solution. Rotate the mixture solution for 20 min. Set the rotating speed at about 4 rpm when a 20-cm diameter holder is used. After mixing, centrifuge the tube for 1 min at 10,000 x *g* to deform the mixed solution.

downstream from the stop codon of Renilla luciferase (pGL4.75[HRuc/CMV]-Bcl2 3′UTR).

3. For reporter assays, transfect 2 µg pGL4.75[HRuc/CMV]-Bcl2 3′UTR using LipofectAMINE™ 2000 (Invitrogen Corp.) into PC-3M-luc cells.
4. Select stable transfectants in hygromycin (0.2 mg/ml; Invitrogen Corp.) using the Dual-luciferase assay-system (Promega). The intensity of Renilla luciferase is normalized by firefly luciferase. Clones expressing both luciferase genes are named PC-3M-luc/Rluc-Bcl2 3′UTR.

3.2. Oligonucleotides Delivery

1. Gently add 600 µl of the oligonucleotide solution to 600 µl atelocollagen solution.
2. Rotate the mixture solution for 20 min. Set the rotating speed at approximately 4 rpm when using a 20-cm diameter holder (see Note 1).
3. After mixing, centrifuge the tube for 1 min at 10,000×*g* to deform the mixed solution (see Note 2). The procedure is shown in Fig. 1.

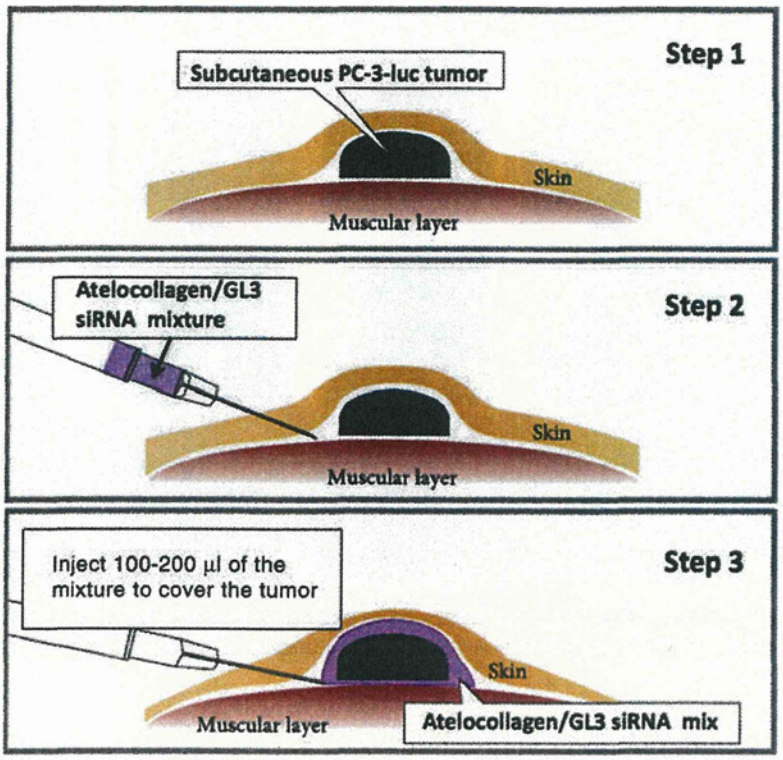

Fig. 2. Administration of the mixture to subcutaneous tumors. Step 1: PC-3-luc subcutaneous tumor; Step 2: insert a 26 G needle subcutaneously approximately 5 mm to the side of the tumor; Step 3: lay the needle parallel to the skin and insert it for 2–3 mm in the direction of the tumor, and then inject the mixture for 20–30 s. It is effective when the mixture is administered so as to cover the whole target site.

3.3. Imaging of Local Delivery of Oligonucleotides

1. Prepare 7- to 10-week-old male athymic nude mice (CLEA Japan, Shizuoka, Japan).
2. To generate a subcutaneous tumor model, the animals are injected with 1×10^6 PC-3-luc cells suspended in 100 ml sterile DPBS.
3. When a tumor develops to 5×5 mm a mixture of GL3 siRNA (specifically knock down firefly luciferase) and atelocollagen are prepared according to the described method.
4. Set the 18-G needle in the disposable syringe and slowly draw the atelocollagen/oligonucleotide mixture (see Note 3).
5. Replace the needle of the syringe with a 26-G injection needle and keep the syringe refrigerated until administration.
6. Insert the injection needle from approximately 5 mm to the side of the subcutaneous tumor with the cut face of the needle turned upward.
7. Lay the needle parallel to the skin and insert it 2–3 mm in the direction of the tumor, and then gently inject 200 µl of the mixture. The procedure is shown in Fig. 2 (see Note 4).

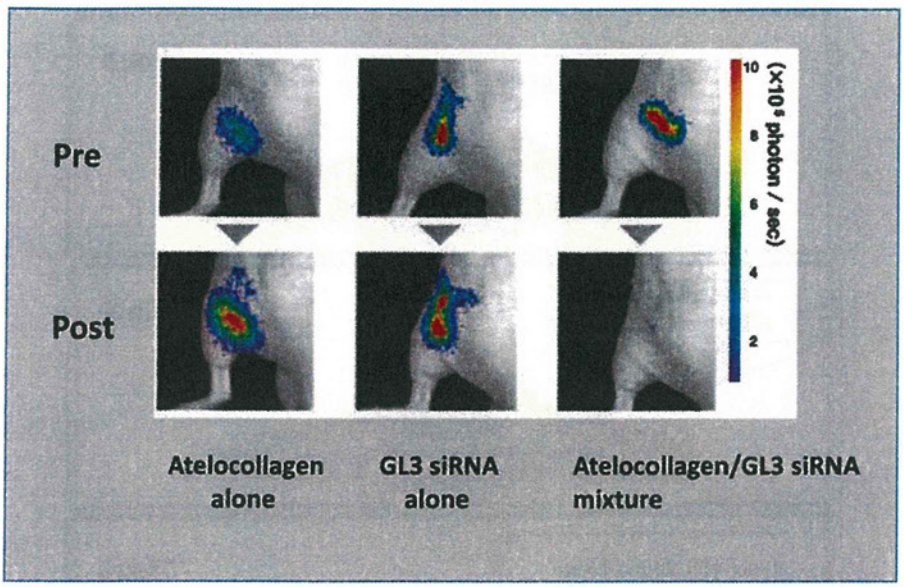

Fig. 3. In vivo imaging of local delivery of oligonucleotides. Firefly luciferase-expressing cells formed subcutaneous tumors. Atelocollagen/GL3 siRNA significantly inhibited the photon count of luciferase as compared to atelocollagen alone and GL3 siRNA alone.

8. 24–48 h after injection (see Note 5), the animals are subjected to bioimaging analysis. An example result is shown in Fig. 3.

3.4. Imaging of Systemic Delivery of Oligonucleotides

1. To generate an experimental metastasis model, the anesthetized animals are injected with 2×10^6 PC-3M-luc cells suspended in 100 ml sterile DPBS into the left heart ventricle (see Note 6).
2. When metastasis develops, a mixture of GL3 siRNA and atelocollagen is prepared according to the above method.
3. Anesthetize the animals, if necessary.
4. Set the 18-G needle in a disposable syringe and slowly draw the atelocollagen/oligonucleotide mixture. In a systemic injection, 100–200 μl of the mixture is used.
5. Replace the syringe needle with the 26-G injection needle and keep the syringe refrigerated until administration.
6. Disinfect the tail of the animal with ethanol.
7. Insert the needle into the vein at a position 1/4 from the tail end.
8. Confirm that the injection needle has entered the vessel and then slowly inject 100–200 μl of the mixture (see Note 7).
9. 24–48 h after injection, the animals are subjected to bioimaging analysis. An example result is shown in Fig. 4.

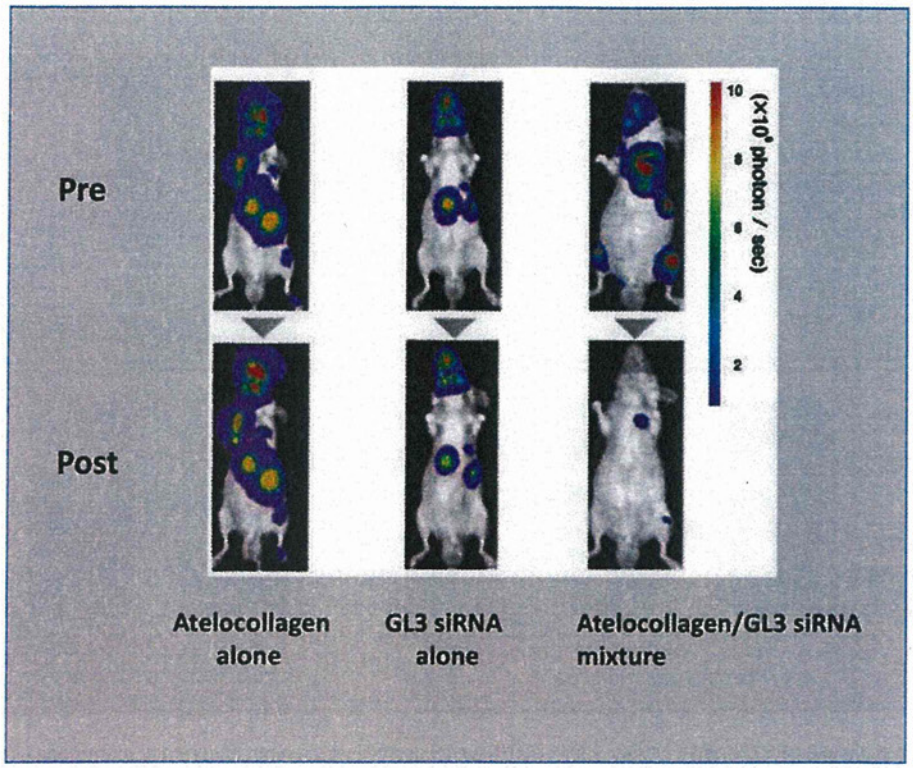

Fig. 4. Firefly-luciferase-expressing cells with formed bone metastasis in mice. Intra-cardiac administration of atelocollagen/GL3 siRNA significantly inhibited the photon count of luciferase as compared to atelocollagen alone and GL3 siRNA alone.

3.5. Dual Luciferase Imaging System for Delivery of Oligonucleotides

1. Seven- to ten-week-old male athymic nude mice (CLEA Japan, Shizuoka, Japan) are anesthetized by exposure to 3% isoflurane on day 0 and subsequent days.
2. On day 0 of the experiments, to generate an experimental metastasis model, the anesthetized animals are injected with 2×10^6 PC-3M-luc/Rluc-Bcl2 3′UTR cells, suspended in 100 ml sterile DPBS, into the left heart ventricle.
3. When metastasis develops, a mixture of miRNA16 and atelocollagen is prepared according to the described method.
4. For systemic injection of the atelocollagen/miRNA mixture, repeat steps 4–8 in Subheading 3.2.
5. For in vivo imaging, the mice are injected with ViviRen (5 mg/kg, Promega) by intravenous tail vein injection and imaged immediately to count the photons from the animal body.
6. After the bioluminescence from Renilla luciferase disappears, the mice are administered D-luciferin (150 mg/kg, Xenogen) by intraperitoneal injection.
7. Ten minutes later, photons from firefly luciferase are counted. An example result is shown in Fig. 5.

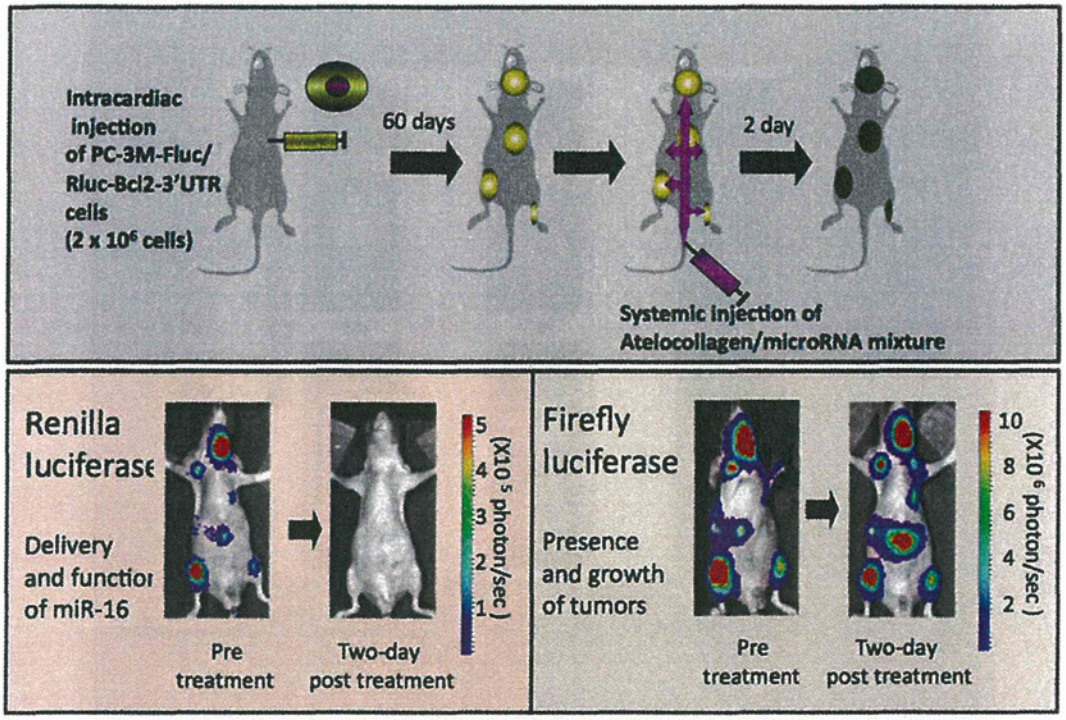

Fig. 5. Dual luciferase cells (PC-3M-Fluc/Rluc-Bcl2-3′UTR) were injected into the heart of mice and formed bone metastases. When the expression of Renilla luciferase from tumor cells could be detected, 50 μg miR-16/atelocollagen was injected intravenously. As can be seen at the bottom of the figure (left side), the photons from the Renilla luciferase were dramatically suppressed one day post-treatment. This result indicates that atelocollagen has the potential for delivering miR-16 throughout the whole body, including bone metastatic sites. Firefly luciferase was not affected, because large-sized tumors like these were not inhibited by a single treatment of miR-16 (29).

4. Notes

1. Avoid mixing by vortexing; otherwise, large aggregates may generate and cause a less efficient delivery of the oligonucleotides.
2. After mixing, ensure there are no visible aggregates.
3. Draw the mixture slowly to avoid incorporation of bubbles.
4. Intratumoral injection is also possible for delivery of atelocollagen/siRNA.
5. The effect of siRNA, such as miRNA delivery by atelocollagen, differs depending on the oligonucleotide sequence, expression level of the target oligonucleotides, the difference in target tumor cells, tissues, site of the tumors, etc. Investigating the

most suitable duration after administration for analysis of gene downregulation is recommended.

6. When the needle is correctly positioned into the left ventricle, bright red oxygenated blood influxes into the needle hub (13, 24). In this model, bone metastases developing in the jaws and/or legs of the mice are detected by non-invasive in vivo bioluminescence imaging.
7. For systemic administration of 200 μl of the mixture, taking 20–30 s will enhance delivery efficacy.
8. In drug resistant tumors, sometimes in vivo bioluminescence imaging does not work well since the luciferin substrate and oligonucleotide mixture are not easily taken up by drug-resistant tumor cells (14).
9. Atelocollagen is a highly purified type I collagen that is modified to have low immunogenicity (Koken, Tokyo). Atelocollagen forms nanosize particles when it is mixed with synthetic miRNAs, via electrostatic binding. The nanoparticles are easily incorporated into cells by endocytosis. The atelocollagen/oligonucleotide complex showed high resistance to nucleases. Therefore, the complex is thought to be stable in vivo (12, 29).
10. It is possible to prepare luciferase-expressing cells with a virus vector system. To generate lentiviral-vector particles containing the luciferase gene, an HIV-1 gag–pol expression plasmid, an HIV-1 Rev expression plasmid and a VSV-G envelope protein expression plasmid were used to package the HIV-based expression vector. In brief, four plasmids were co-transfected into 293FT cells. Two days after transfection, the supernatants were cleared from the cellular debris by low-speed centrifugation (10 min, 1,000 × *g*) and filtration through 0.45-μm filters. Aliquots were stored at −80°C.

Acknowledgements

This work was supported in part by a Grant-in-Aid for the Third-Term Comprehensive 10-Year Strategy for Cancer Control, a Grant-in-Aid for Scientific Research on Priority Areas Cancer from the Ministry of Education, Culture, Sports, Science and Technology, and the Program for Promotion of Fundamental Studies in Health Sciences of the National Institute of Biomedical Innovation (NiBio), and a Takeda Science Foundation.

References

1. Bass, B.L. (2000) Double-stranded RNA as a template for gene silencing. *Cell* **101**, 235–238.
2. Mcmanus, M.T. and Sharp, P.A. (2003) Gene silencing in mammals by small interfering RNAs. *Nat Rev Genet* **3**, 737–747.
3. Shankar, P., Manjunath, N., and Lieberman, J. (2005) The prospect of silencing disease using RNA interference. *JAMA* **293**, 1367–1373.
4. Leung, R.K., Whittaker, P.A. (2005) RNA interference: from gene silencing to gene-specific therapeutics. *Pharmacol Ther* **107**, 222–239.
5. Behlke, M.A. (2006) Progress towards in vivo use of siRNAs. *Mol Ther* **13**, 644–670.
6. Dykxhoorn, D.M., Palliser, D., and Lieberman, J. (2006) The silent treatment: siRNAs as small molecule drugs. *Gene Ther* **13**, 541–552.
7. Rayburn, E.R., Wang, H., and Zhang, R. (2006) Antisense-based cancer therapeutics: are we there yet? *Expert Opin Emerg Drugs* **11**, 337–352.
8. Hagan, J.P. and Croce, C.M. (2007) MicroRNAs in carcinogenesis. *Cytogenet Genome Res* **118**, 252–259.
9. Jiang, J., Gusev, Y., Aderca, I., Mettler, T.A., Nagorney, D.M., Brackett, D.J., Roberts, L.R., and Schmittgen, T.D. (2008) Association of microRNA expression in hepatocellular carcinomas with hepatitis infection, cirrhosis, and patient survival. *Clin Cancer Res* **14**, 419–427
10. Bartel, D.P. (2004) MicroRNAs: genomics, biogenesis, mechanism, and function. *Cell* **116**, 281–297.
11. Osaki, M., Takeshita, F., and Ochiya, T. (2008) MicroRNA as biomarkers and therapeutic drugs in human cancer. *Biomarkers* **13**, 658–670.
12. Minakuchi, Y., Takeshita, F., Kosaka, N., Sasaki, H., Yamamoto, Y., Kouno, M., Honma, K., Nagahara, S., Hanai, K., Sano, A., Kato, T., Terada, M., and Ochiya, T. (2004) Atelocollagen-mediated synthetic small interfering RNA delivery for effective gene silencing in vitro and in vivo. *Nucleic Acids Res* **32**:e109.
13. Takeshita, F., Minakuchi, Y., Nagahara, S., Honma, K., Sasaki, H., Hirai, K., Teratani, T., Namatame, N., Yamamoto, Y., Hanai, K., Kato, T., Sano, A., and Ochiya, T. (2005) Efficient delivery of small interfering RNA to bone-metastatic tumors by using atelocollagen in vivo. *Proc Natl Acad Sci USA* **102**, 12177–12182.
14. Honma, K., Iwao-Koizumi, K., Takeshita, F., Yamamoto, Y., Yoshida, T., Nishio, K., Nagahara, S., Kato, K., and Ochiya, T. (2008) *RPN2* gene confers docetaxel resistance in breast cancer. *Nat Med* **14**, 939–948.
15. Takei, Y., Kadomatsu, K., Goto, T., and Muramatsu, T. (2006) Combinational antitumor effect of siRNA against midkine and paclitaxel on growth of human prostate cancer xenografts. *Cancer*, **107**, 864–873.
16. Vooijs, M., Jonkers, J., Lyons, S., and Berns, A. (2002) *Cancer Res* **62**, 1862–1867.
17. Hoffman, R.M. (1999) Orthotopic transplant mouse models with green fluorescent protein-expressing cancer cells to visualize metastasis and angiogenesis. *Cancer and Metastasis Reviews* **17**, 271–277.
18. Hoffman, R.M. (1999) Orthotopic metastatic mouse models for anticancer drug discovery and evaluation: a bridge to the clinic. *Invest New Drugs* **17**, 343–359.
19. Hoffman, R.M. (2002) In vivo imaging of metastatic cancer with fluorescent proteins. *Cell Death Differ* **9**, 786–789.
20. Hoffman, R.M. (2005) Orthotopic metastatic (MetaMouse) models for discovery and development of novel chemotherapy. *Methods Mol Med* **111**, 297–322.
21. Nakanishi, H., Ito, S., Mochizuki, Y., and Tatematsu, M. (2005) Evaluation of chemosensitivity of micrometastases with green fluorescent protein gene-tagged tumor models in mice. *Methods Mol Med* **111**, 351–362.
22. Hennig, R., Ventura, J., Segersverd, R., Ward, E., Ding, X.Z., Rao, S.M., Jovanovic, B.D., Iwamura, T., Talamonti, M.S., Bell, R.H. Jr, and Adrian, T.E. (2005) LY293111 improves efficacy of gemcitabine therapy on pancreatic cancer in a fluorescent orthotopic model in athymic mice. *Neoplasia* **7**, 417–425.
23. Contag, P.R., Olomu, I.N., Stevenson, D.K., and Contag, C.H. (1998) Bioluminescent indicators in living mammals. *Nat Med* **4**, 245–247.
24. Rehemtulla, A., Stegman, L.D., Cardozo, S.J., Gupta, S., Hall, D.E., Contag, C.H., and Ross, B.D. (2000) Rapid and quantitative assessment of cancer treatment response using in vivo bioluminescence imaging. *Neoplasia* **2**, 491–495.
25. Jenkins, DE, Oei, Y, Hornig, YS, Yu, S.F., Dusich, J., Purchio, T., and Contag, P.R. (2003) Bioluminescent imaging (BLI) to improve and refine traditional murine models of tumor growth and metastasis. Clin Exp Metastasis **20**, 733–744.

26. Vooijs, M., Jonkers, J., Lyons, S., and Bernes, A. (2002) Noninvasive imaging of spontaneous retinoblastoma pathway-dependent tumors in mice. *Cancer Res* **62**, 1862–1867.
27. Lyons, S.K. (2005) Advances in imaging mouse tumor models in vivo. *J Pathol* **205**,194–205.
28. Laurie, N.A., Gray, J.K., Zhang, J., Leggas, M., Relling, M., Egorin, M., Stewart, C., and Dyer, M.A. (2005) Topotecan combination chemotherapy in two new rodent models of retinobrastoma. *Clin Cancer Res* **11**, 7569–7578.
29. Takeshita, F., Bader, A.G., Osaki, M., Takahashi, R., Yamamoto, Y., Kosaka, N., Kawamata, M., Kelnar, K., Brown, D., and Ochiya, T. (2010) Systemic delivery of miR-16 for RNAi therapy in prostate cancer. *Mol Ther* **18**, 181–187.

SCIENTIFIC REPORTS

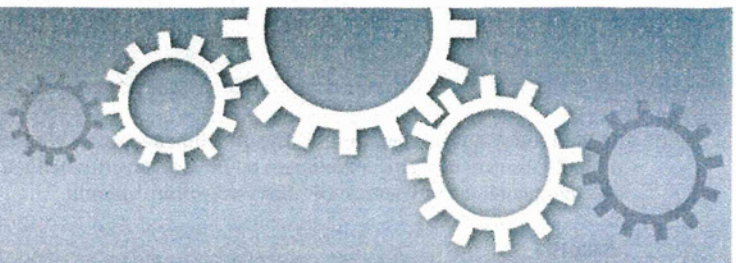

OPEN

SUBJECT AREAS:
PLURIPOTENCY
EMBRYONIC STEM CELLS
CANCER MODELS
MECHANISMS OF DISEASE

Received
17 July 2012

Accepted
29 October 2012

Published
10 December 2012

Correspondence and requests for materials should be addressed to T.O. (tochiya@ncc.go.jp)

Two distinct knockout approaches highlight a critical role for p53 in rat development

Masaki Kawamata & Takahiro Ochiya

Division of Molecular and Cellular Medicine, National Cancer Center Research Institute, 1-1, Tsukiji, 5-chome, Chuo-ku, Tokyo 104-0045, Japan.

Gene targeting in embryonic stem cells (ESCs) has become the principal technology for generating knockout models. Although numerous studies have predicted that the disruption of *p53* leads to increased developmental anomalies and malignancies, most *p53* knockout mice develop normally. Therefore, the role of *p53* in animal development was examined using rat knockout models. Conventionally generated homozygous KO males developed normally, whereas females rarely survived due to neural tube defects. Mutant chimeras generated via blastocyst injection with *p53*-null ESCs exhibited high rates of embryonic lethality in both sexes. This phenotype could be observed in one month by the use of zinc-finger nucleases. The *p53*-null ESCs were resistant to apoptosis and differentiation, and exhibited severe chromosome instabilities in the chimera-contributed cells, suggesting an essential role for p53 in maintaining ESC quality and genomic integrity. These results demonstrate that p53 functions as a guardian of embryogenesis in the rats.

Over the past two decades, knockout (KO) technology in mice has helped to clarify the physiological function of a large number of genes. However, unexpected phenotypes have been observed in some cases, making it difficult to understand the role of the deleted gene, or to translate that data to the phenotypes of human diseases caused by mutations in such genes. Thus, gene-targeting techniques for other animals, such as rats, have long been sought. Many strategies for manipulating rat genes to generate loss-of-function models have been adapted from the mouse genetic toolbox, including conventional transgenesis by pronuclear injection[1], RNA interference[2], N-ethyl-N-nitrosourea (ENU) mutagenesis[3,4], and transposon mutagenesis[5–7]. KO rats have been produced using Zinc-finger nuclease (ZFN) technology[8,9], and, most recently, germline-competent rat ESCs and rat induced pluripotent stem cells (iPSCs) have been established by the addition of cell-signaling inhibitors to the culture medium[10–13], making it possible to generate both transgenic (Tg)[12,14] and KO rats[15].

The tumor suppressor gene *p53* is a good example of a gene whose function in mouse development requires further scrutiny. Donehower et al. first reported normal Mendelian ratios and postnatal development in *p53* homozygous KO mice[16]. However, two other groups later showed that a fraction of homozygous KO females had fatal embryonic exencephaly, a defect in neural tube closure that results in an overgrowth of neural tissue in the midbrain region[17,18]. Such results indicate that, at least in some cases, p53 influences development in females[19]. In the case of *p53* homozygous KO rats, neural tube defects (NTDs) in females were not found but increased susceptibility to tumor development was reported[15,20,21].

p53 has been shown to regulate not only cell cycle arrest, apoptosis, and DNA repair in many types of cells[22], but also stemness, by suppressing *Nanog* expression in ESCs[23]. Considering these observations, malignant transformations may occur in *p53*-null ESCs and chimera development may be hindered. However, chimeric mutant mice have been successfully generated via the injection of blastocysts with iPSCs derived from *p53*-null mouse embryonic fibroblasts (MEFs), and germline transmission of the *p53*-null cells was also accomplished[24,25]. The properties of rat ESCs differ from those of mouse ESCs in that rat ESCs cannot be cultured in mouse ESC culture conditions due to their high sensitivity to differentiation signals[26]. Thus, an approach using *p53*-null rat ESCs might reveal new insights into the function of p53 in regulating stemness and animal development.

We previously generated *Oct4*-Venus Tg rats, and established *Oct4*-Venus ESC lines in which *Oct4* expression can be monitored by green fluorescence[12,27]. Here, both conventionally KO and mutant chimeras rats were generated using *p53*-null *Oct4*-Venus ESCs, and their development was investigated. Moreover, an efficient

method for a rapid generation of mutant chimeras was developed using ZFN-mediated gene targeting in rat ESCs. Using this method, developmental phenotypes can be observed within 1 month.

Results

Conventionally generated $p53^{-/-}$ females reveal the cause of NTDs. *p53* homozygous KO rats were generated via germline transmission of heterozygous $p53^{+/C}$ ESCs (Fig. 1a,b,e). The details are described in the *Materials and Methods*. The Mendelian ratios in weaned rats produced from heterozygous intercrosses were investigated (Fig. 2a). The frequency of homozygous $p53^{C/C}$ rats was 16.9%, less than the anticipated value of 25% (Table 1). Moreover, only one $p53^{C/C}$ female developed normally, frequency = 0.70%, significantly less than 16.2% $p53^{C/C}$ males. These results suggest that most of the $p53^{C/C}$ females either do not survive gestation, or die after birth but prior to weaning. To investigate the developmental dysfunctions in $p53^{C/C}$ females, litters from heterozygous intercrosses were examined at embryonic day 16.0 (E16.0) to E18.0. Eleven $p53^{C/C}$ female embryos (12.8%, 11/86) were recovered at this stage; six (57%, 6/11) exhibited exencephaly (Table 1) and two of these also exhibited spina bifida (Fig. 2b). Although these two abnormalities are the most prevalent NTDs, spina bifida in *p53* mutant mice has only been reported in one study[28]. Exencephaly was only found in the female embryos, consistent with previous observations of a higher incidence of NTDs in human females and in numerous mouse models[29]. Expression of SOX2, a marker for primordial neuronal cells

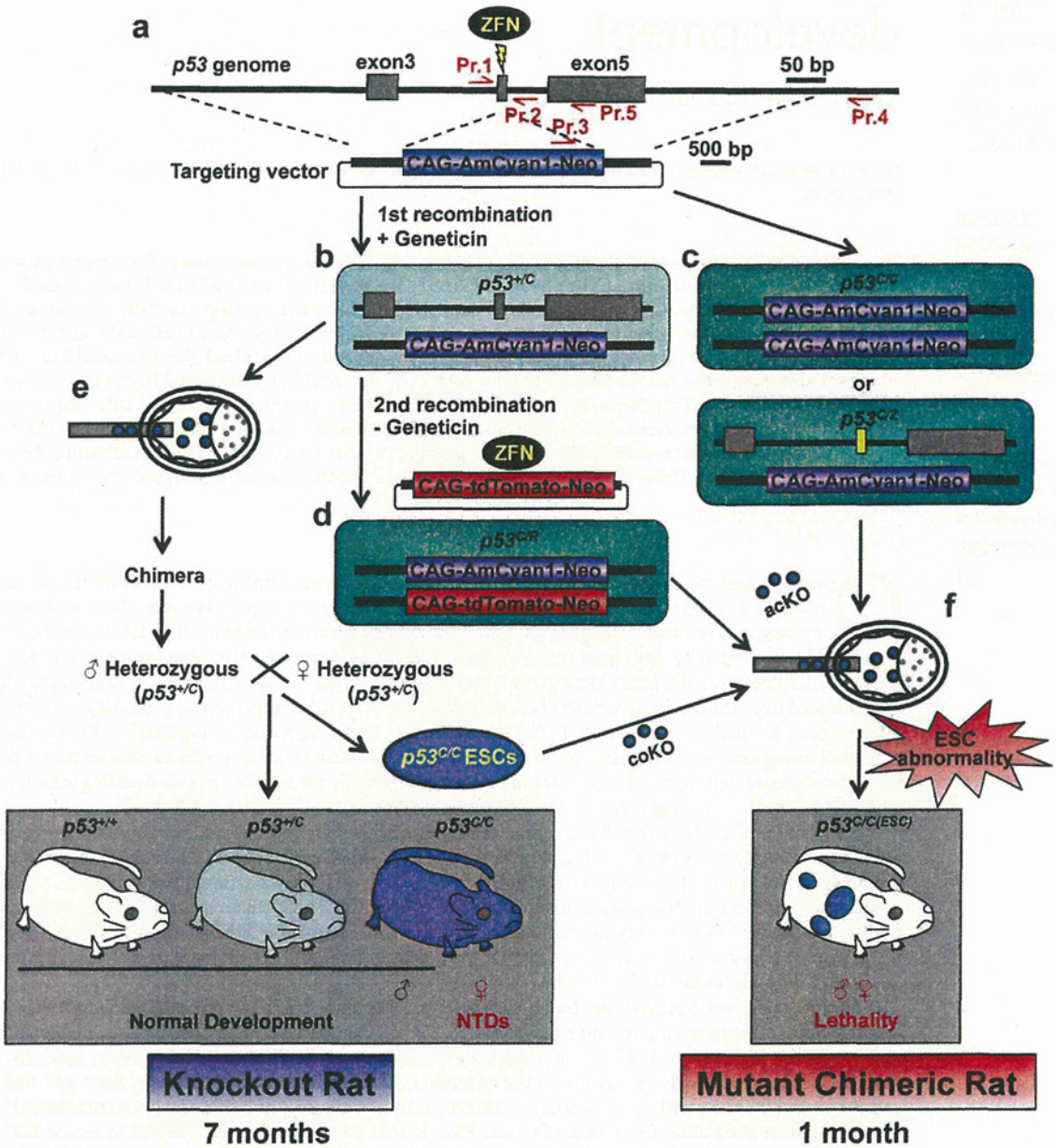

Figure 1 | Schematic representation of *p53* KO strategy in rats. (a–d) Both mono- (b) and bi-allelic (c) or 2ndary (d) homologous recombination are induced by ZFN. (e, f) Heterozygous or homozygous ESC-injection leads to the generation of conventionally generated KO model (e) or ESC-based mutant chimeric models (f), respectively. A yellow box indicates a frame shift mutation induced by ZFNs. Pr., Primer. coKO, congenital KO. acKO, acquired KO.

Table 1 | The *p53* Genotypes of Adult and Embryonic Rats

Genotype	$p53^{+/+}$	$p53^{+/C}$	$p53^{C/C}$	$p53^{C/C}$ Exencephaly
Adults	41 (28.9%)	77 (54.2%)	24 (16.9%)	0
Male	18 (12.7%)	42 (29.6%)	23 (16.2%)	0
Female	23 (16.2%)	35 (24.6%)	1 (0.70%)	0
Embryos	21 (24.4%)	48 (55.8%)	17 (19.8%)	6
Male	11 (12.8%)	22 (25.6%)	6 (7.0%)	0
Female	10 (11.6%)	26 (30.2%)	11 (12.8%)	6 (54.5%)[a]

[a]Of the 11 $p53^{C/C}$ female embryos, six exhibited exencephaly.

expressed in the embryonic neural plate[30], was detected on the surface of the brain and in areas of spina bifida (Fig. 2d, arrowheads), confirming that neural tube closure had failed. Compared to a $p53^{+/C}$ embryo (Fig. 2e, right), the aberrant ventricular zone (VZ) structure in the brain of a $p53^{C/C}$ exencephalic embryo was revealed by the localization of SOX2 (Fig. 2d left, arrows), which is expressed in the neuroendothelial stem cells of the VZ[31]. In this embryo, *Oct4*-Venus expressing cells were aberrantly located in the exencephalic region (Fig. 2b, green square, and 2c).

Embryonic lethality in a mutant chimeric model. ZFNs can create site-specific double-strand breaks, which are repaired via non-homologous end joining, resulting in frame-shift mutations by the arbitrary addition or deletion of base pairs. Cotransfection of ZFNs with targeting vectors enhances homologous recombination, not only in human pluripotent cells[32,33], but also in one-cell embryos, leading to the direct generation of knock-in mice[34] and rats[35]. In the present work, ZFNs were used to produce homozygous mutant ESC lines by a single recombination step (Fig. 1c). Using this approach, 1 of 46 (2.2%) clones harbored dual knock-in alleles ($p53^{C/C}$), while 7 of 46 (15%) clones possessed both knock-in and frame shift mutant alleles ($p53^{C/Z}$). In a 2nd-step recombination, homozygous clones were also produced from a $p53^{+/C3}$ ESC clone based on the same strategy using both ZFNs and a targeting vector expressing red fluorescence (Fig. 1b,d). A successful homologous recombination was achieved in 3 of 8 clones (38%, $p53^{C/R}$; Supplementary Fig. S2c). These ESC lines were called acquired KO (acKO) ESCs (Fig. 1c). The contribution of $p53^{-/-}$ ($p53^{C/C}$, $p53^{C/Z}$, or $p53^{C/R}$) ESCs to rats, which are called $p53^{-/-\,(ESC)}$ rats, was examined, and the timeline for the rapid generation of the mutant chimeras is shown schematically (Fig. 3a,b). Microinjection of $p53^{-/-}$ ESCs into blastocysts led to the delivery of only a few pups (0.4 ± 0.2 per foster mother, n=5, 4 cell lines). This number (0.4 ± 0.2/foster mother) was significantly smaller than the number of pups delivered following injection of $p53^{+/+}$ ESCs into blastocysts (4.0 ± 1.1 per foster mother, n=5, 3 cell lines, $P<0.05$) or $p53^{+/-}$ ($p53^{+/C}$) ESCs (5.1 ± 1.1 per foster mother, n=9, 4 cell lines, $P<0.05$) (Fig. 3c). The

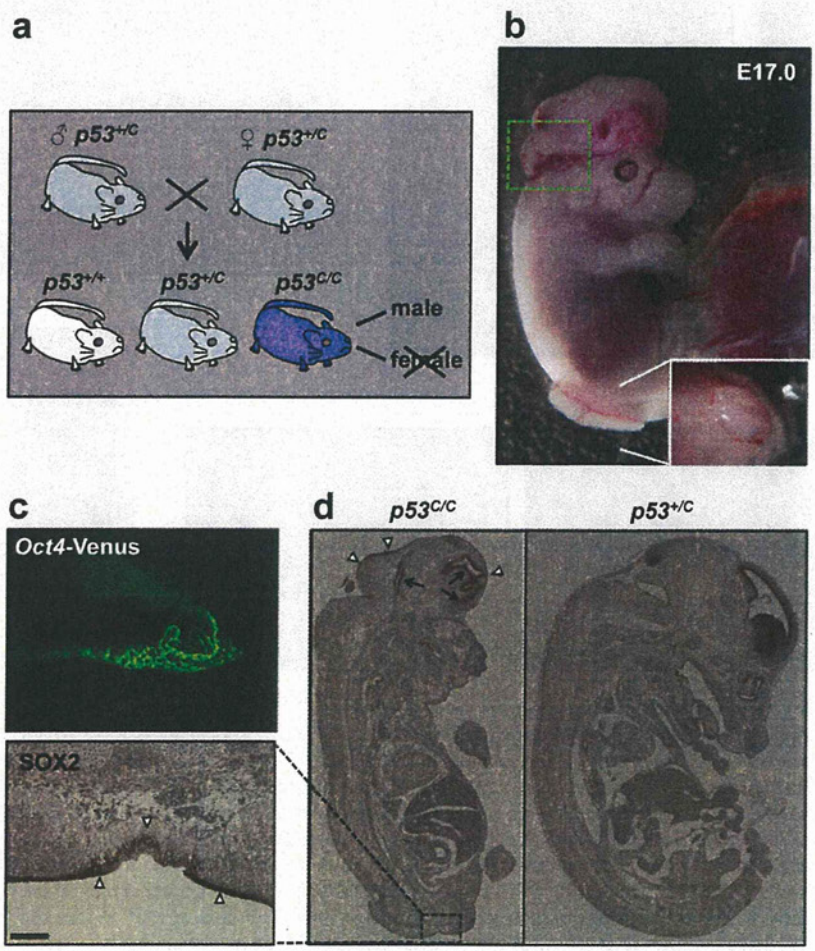

Figure 2 | Phenotypes in conventionally generated p53 homozygous rats. (a) Schematic representation of heterozygous intercrosses indicates a loss of adult female. (b) An embryo at day 17.0 of gestation (E17.0) displaying exencephaly and spina bifida. A dotted green square indicates (c). (c) Fluorescence image of the area inside the dotted green square in (b). *Oct4*-Venus fluorescence is observed in the exencephalic region. (d) IHC staining for SOX2 identifies positive cells in the ventricular zone (arrows) and surface (arrowheads) of both brain and spina bifida (magnified image, scale bar = 100 μm).

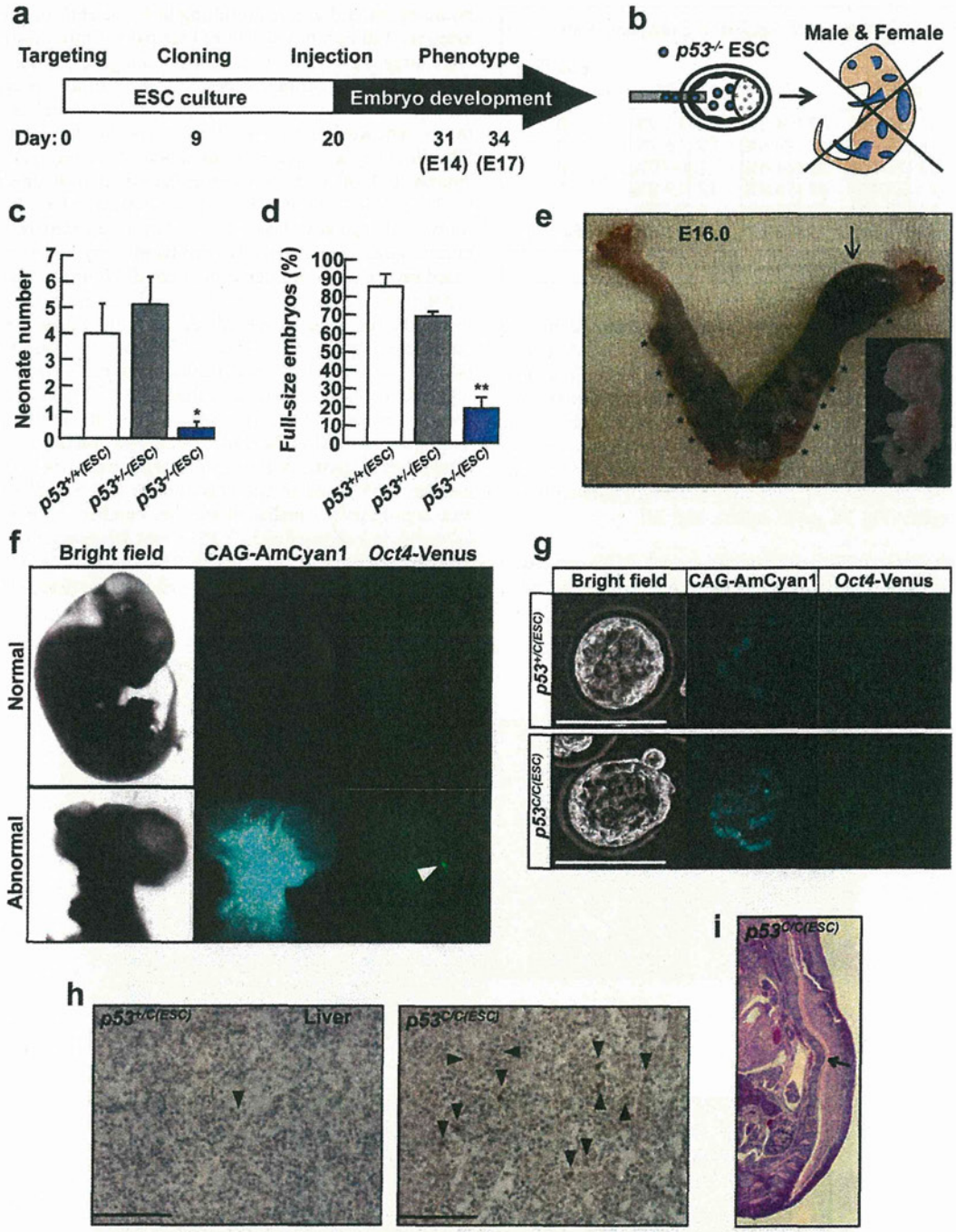

Figure 3 | Embryonic lethality in p53 mutant chimeras. (a) Time line for generating $p53^{-/-\,(ESC)}$ chimeras and (b) Schematic representation to investigate phenotype during embryogenesis. (c) Number of neonates successfully delivered. $p53^{+/+}$ (n=5, 3 cell lines), $p53^{+/-}$ (n=9, 4 cell lines) or $p53^{-/-}$ (n=5, 4 cell lines) ESCs were injected into wild-type blastocysts. n, injection number. *, $P<0.05$, $p53^{-/-}$ vs. $p53^{+/+}$ and $p53^{+/-}$. (d) The ratio of chimeric embryos with normal body size at E14.0 to E17.0. $p53^{+/+}$ (n=4, 4 cell lines), $p53^{+/-}$ (n=7, 4 cell lines) or $p53^{-/-}$ (n=14, five cell lines) ESCs were injected into wild-type blastocysts. n, injection number. **, $P<0.001$, $p53^{-/-}$ vs. $p53^{+/+}$ and $p53^{+/-}$. (e) Developmental dysfunction in chimeric embryos injected with $p53^{C/R2}$ ESCs at E16.0. An arrow indicates a chimera with growth retardation (inset). Asterisks indicate fetal absorption. (f) Correlation between developmental dysfunction and ESC contribution. $p53^{C/C1}$ ESCs expressing AmCyan1 contribute to chimeric embryos at E14.0. An arrowhead indicates an ectopic expression of *Oct4*-Venus. (g) $p53^{C/R4}$ ESC proliferation in blastocyst. Twelve ESCs were injected into blastocyst, followed by incubation overnight in YPAC medium. (h) Immunohistochemistry using Cleaved-Caspase3 antibody in liver of $p53^{+/C(ESC)}$ or $p53^{C/C(ESC)}$ chimera. Arrowheads indicate the apoptotic cells. (i) Spinal curvature (an arrow) in $p53^{C/C(ESC)}$ chimera. All scale bars = 100 μm.

newborns derived from $p53^{-/-}$ ESC-injections did not exhibit a brown coat-color, indicating that they were not chimeras. Because these results suggest that the development of $p53^{-/-\,(ESC)}$ embryos was defective, fetal development at stages E14.0 to E17.0 was examined. Approximately 80% of the $p53^{-/-\,(ESC)}$ embryos (n=14, 5 cell lines, Fig. 3d) showed abnormal development resulting in complete

resorption (Fig. 3e, asterisks) or growth retardation (Fig. 3e, an arrow and inset). A large number of $p53^{-/-}$ ESC-derived cells were detected in these embryos (Fig. 3f, lower). However, the remaining $p53^{-/-\,(ESC)}$ embryos (30/189 embryos: 20.0 ± 5.6%) developed a normal body size (Fig. 3f, upper and Supplementary Table S1). The number of normal embryos (20.0 ± 5.6%) was significantly lower than that of $p53^{+/+(ESC)}$ embryos (53/63 embryos: 85.1 ± 5.8%, n=4, 4 cell lines, $P<0.01$) or $p53^{+/-(ESC)}$ embryos (44/64 embryos: 69.0 ± 2.2%, n=7, 4 cell lines, $P<0.01$) (Fig. 3d). Among the normal-sized $p53^{-/-(ESC)}$ embryos, 26 of 30 (87.8 ± 9.7%, n=10, 5 cell lines) embryos were chimeras, whereas 22 of 26 displayed a relatively lower contribution of the mutant cells. Although the number of $p53^{+/-(ESC)}$ chimera (30/44 embryos, 66.9 ± 6.6%, n=7, 4 cell lines) was similar to that of $p53^{-/-(ESC)}$ chimera ($P=0.14$), the $p53^{+/-(ESC)}$ chimeras developed normally (Fig. 3c, d). The number of $p53^{+/+(ESC)}$ chimera (17/53 embryos, 36.0 ± 10.2%, n=4, 4 cell lines) was significantly smaller than that of either $p53^{+/-(ESC)}$ ($P=0.044$) or $p53^{-/-(ESC)}$ ($P=0.0081$) chimera. These results suggest that *p53* mutation enhances the chimeric contribution of ESCs and the high contribution of *p53*-null ESCs induces embryonic lethality.

To address the mechanisms by which $p53^{-/-}$ ESCs result in embryonic lethality, the behavior of $p53^{-/-}$ ESCs was followed in blastocysts incubated *in vitro*. Blastocysts were injected with 12 ESCs and incubated over night. Although $p53^{+/+1}$ ESCs remained in the blastocysts, the number decreased to 4.0 ± 0.89 cells (Fig. 3g, upper, n=5). In contrast, a significantly larger number of $p53^{C/R4}$ ESCs (13.7 ± 1.2 cells, n=7, $P<0.0001$) were detected (Fig. 3g, lower), indicating proliferation of the *p53*-null ESCs in the blastocysts. The excess proliferation may lead to a high ESC contribution, resulting in the developmental abnormalities that led to resorption of the fetuses. In fact, several of the $p53^{C/C(ESC)}$ chimeras with normal body size displayed increased number of apoptotic cells in the liver (Fig. 3h, arrowheads) and one chimera exhibited an abnormal spinal curvature (Fig. 3i, an arrow). Embryos such as these may die and undergo resorption before birth, resulting in the significant loss of neonates as shown in Figure 3d.

Morphology and global gene expression profile in $p53^{-/-}$ ESCs. The properties of $p53^{-/-}$ ESCs were examined. Venus-negative differentiated cells (Fig. 4a, left, arrowheads) survived the processes of cloning and passaging $p53^{-/-}$ Venus-positive ESCs (Fig. 4a, left, arrows), indicating that $p53^{-/-}$ differentiated cells escaped from apoptosis. Rat ESC colonies adopt a dome-shaped morphology and tend to detach from culture dishes coated with MEFs[12,15]. The $p53^{-/-}$ domed colonies were detached by pipetting and the cells were passaged after dissociation, leading to successful propagation of dome-shaped colonies; no differentiated cells were detected. (Fig. 4a, right, arrows). The morphology of the $p53^{-/-}$ lines was

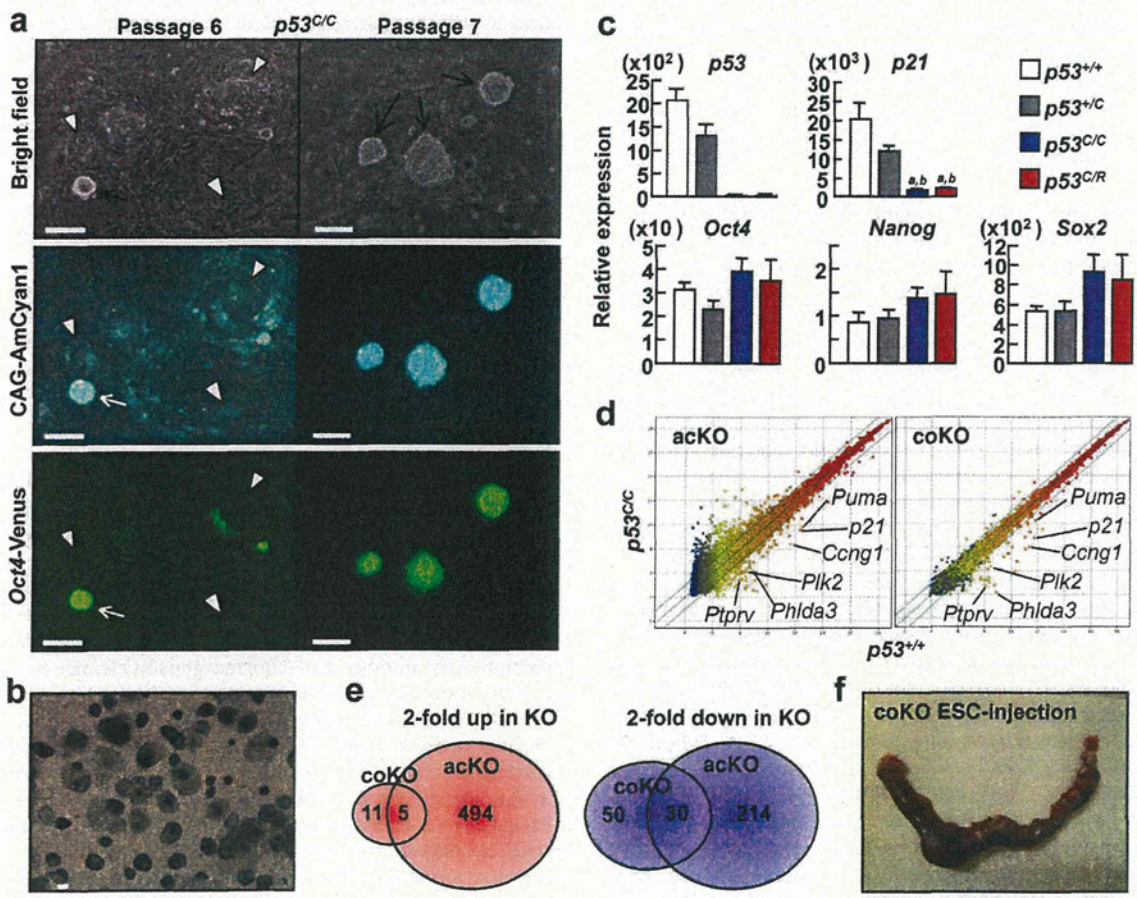

Figure 4 | Characteristics of *p53*-null ESCs. (a) A $p53^{C/C1}$ ESC clone is shown. Arrows indicate pluripotent colonies. Arrowheads indicate differentiated cells. (b) ALP staining in $p53^{C/C1}$ ESCs. (c) q-PCR analysis in *p53* mutant ESCs. Transcript levels were normalized to *Gapdh* levels. Data are the mean ± SD of one biological sample assayed in four independent experiments. *a*, $P<0.05$ versus $p53^{+/+}$; *b*, $P<0.005$ versus $p53^{+/C}$. (d) Scatter plots of global gene expression microarrays comparing $p53^{+/+}$ and $p53^{C/C}$ ESCs of an acKO (left) or coKO (right) line. The green lines delineate the boundaries of a 2-fold difference in gene expression levels. (e) Venn diagrams of the intersection between genes highly (left) or lowly (right) expressed in the coKO versus the acKO in $p53^{C/C}$ ESCs. (f) Developmental dysfunction in chimeric embryos injected with $p53^{C/C2}$ coKO ESCs at E16.0. All scale bars = 100 μm.

indistinguishable from that of $p53^{+/-}$ or $p53^{+/+}$ cells (Supplementary Fig. S3). The $p53^{C/C}$ ESCs were positive for alkaline phosphatase (ALP) activity (Fig. 4b).

The expression levels of ESC marker genes, such as *Oct4*, *Nanog* and *Sox2*, were similar in $p53^{C/C}$ and $p53^{C/R}$ ESCs compared to $p53^{+/+}$ or $p53^{+/C}$ cells, whereas loss of *p53* mRNA and parallel reduction in the mRNA level of the *p53* target gene *p21* were confirmed in mutant ESC lines (Fig. 4c). The ESC line produced by acquired gene targeting in wild-type ESCs ('acKO' ESCs) and a congenital KO ESC line derived from heterozygous intercrosses (named coKO) were analyzed to determine whether some compensatory effect occurred in the coKO line. A microarray analysis showed that the coKO line had less divergent expression compared to the acKO line (acKO vs. coKO: 494 vs. 11 genes upregulated and 214 vs. 50 genes downregulated, Fig. 4e). Venn diagrams showing the overlap in genes identified in the two KO ESC datasets identified only five upregulated and 30 downregulated genes (Fig. 4e, and see Supplementary Table S2). Many of the downregulated genes in the $p53^{C/C}$ ESCs were direct targets of *p53*, such as *Puma*, *p21*, *Ccng1*, *Plk2*, *Phlda3*, and *Ptprv* (Fig. 4d), whereas no genes for pluripotency or stemness were identified.

Chimera generation was used to investigate whether microinjection with these coKO ESCs could rescue mutant chimera development. Male ESC lines were also examined because homozygous males showed normal development. However, microinjection of both female cell lines (n=4, 2 cell lines) and male coKO ESC cell lines (n=7, 3 cell lines) produced chimeras in which embryogenesis failed, similar to the acKO chimeras (Fig. 4f and Supplementary Table S1). The fraction of full-sized embryos (15/68 embryos: 23.1 ± 4.0%, n=9, 5 cell lines) was similar to that of acKO chimeras (30/189 embryos: 20.0 ± 5.6%, n=14, 5 cell lines). These results indicate that lethality in mutant chimeras is due to abnormality of $p53^{-/-}$ ESCs.

$p53^{-/-}$ ESCs are resistant to apoptosis and differentiation. To investigate susceptibility to apoptosis, flow cytometry to detect surface exposure of Annexin V was performed in ESCs under routine culture conditions using YPAC medium [Y, Y-27632 (ROCK inhibitor); P, PD0325901 (MEK inhibitor); A, A-83-01 (TGF-β inhibitor); C, CHIR99021 (GSK3 inhibitor)][12]. A control treatment with G418 caused an increase in Annexin V-positive apoptotic cells whereas each of the *p53* genotype ESCs exhibited small population of the apoptotic cells ($p53^{+/+}$, 11.0 ± 0.25%; $p53^{+/C}$, 14.0 ± 0.30%; $p53^{C/C}$, 11.0 ± 0.49%) (Fig. 5a). Assays for colony formation and embryoid body (EB) formation were performed under differentiation culture conditions to examine the behavior of the mutant ESCs. There was no genotype-dependent difference in the numbers of undifferentiated or differentiated colonies under conditions using YPAC medium and MEFs (Fig. 5b). Under culture conditions using Y media and MEFs (inhibitors P, A and C were absent, Fig. 5c), almost no $p53^{+/+}$ undifferentiated colonies formed (1.7 ± 0.9 colonies) but some $p53^{+/C}$ colonies were observed (13.0 ± 2.1 colonies, $P<0.01$). Few differentiated colonies of either genotype were formed. In contrast, $p53^{C/C}$ cells formed a large number of both undifferentiated (56.0 ± 2.6 colonies, $P<0.0001$ vs. $p53^{+/+}$; $P<0.001$ vs. $p53^{+/C}$) and differentiated (26.3 ± 1.5 colonies, $P<0.0001$ vs. $p53^{+/+}$; $P<0.0001$ vs. $p53^{+/C}$) colonies (Fig. 5c). These results suggest that $p53^{-/-}$ ESCs strongly maintain both undifferentiated state and self-renewal capacities while the differentiated cells are protected from apoptosis, consistent with the results shown in Figure 3a. Next, colony formation was assessed under culture conditions in which ESCs weakly attach to un-coated culture dishes in the absence of MEFs. Although undifferentiated colony formation was rare in both $p53^{+/+}$ (11.3 ± 3.5) and $p53^{+/C}$ (2.0 ± 1.2) ESCs, a large number of $p53^{C/C}$ ESCs formed colonies (96.7 ± 2.8 colonies, $P<0.0001$ vs. $p53^{+/+}$; $P<0.0001$ vs. $p53^{+/C}$; Fig. 4d). In the un-coated dishes in the absence of MEFs, differentiated colonies were rarely formed from any ESC genotype. Thus, the $p53^{-/-}$ ESCs might have an increased capacity to adhere tightly to the culture dish and/or proliferate without the support of feeder cells.

When EB formation was examined, $p53^{+/+}$ EBs formed by day 3 underwent apoptosis over time in culture, resulting in few EBs remaining by day 7 relative to day 3. In addition, Venus fluorescence was completely lost in these cells (Fig. 5e, left). In contrast, $p53^{C/C}$ EBs were large in size and number, and maintained Venus fluorescence (Fig. 5e, right). The number of cells in $p53^{C/C}$ EBs (3.25×10^5) was significantly larger than cell number in $p53^{+/+}$ EBs (1.00×10^3, $P<0.01$) or $p53^{+/C}$ EBs (2.47×10^4, $P<0.01$). Moreover, these data indicate that $p53^{C/C}$ EBs actively proliferated because the cell number increased from 2.5×10^5 at day 0 to 3.25×10^5 by day 7 (Fig. 5f). This result suggests that $p53^{C/C}$ cells are able to proliferate even in the absence of cell attachment. $p53^{+/C}$ EBs showed an intermediate phenotype with significant differences from the other genotypes ($P<0.01$ vs. $p53^{+/+}$, $P<0.01$ vs. $p53^{C/C}$).

Chromosomal instability in $p53^{-/-}$ cells. Next, karyotype analysis was performed in $p53^{-/-}$ cells. Although $p53^{+/C}$ ESCs maintained a normal karyotype 42,XX,[20], one $p53^{C/R2}$ ESC clone exhibited abnormal karyotype 42,XX,add(15)(q22)[20] (Fig. 6a, red square and arrow). Moreover, once the $p53^{C/R2}$ ESC clone differentiated under EB forming culture conditions for two weeks (Fig. 6b), an additional chromosomal aberration, 41,X,-X,add(15)(q22)[20], was found in all cells analyzed (Fig. 6a, blue square). In a $p53^{C/C1}$ ESC clone, ESCs did not have an abnormal karyotype (42,XX[20]). However, cells derived from the $p53^{C/C1(ESC)}$ chimera in E14.0 rats displayed various chromosomal aberrations, such as 42,XX,add(1)(q52)[1], 42,XX,add(3)(p12) [1], 43,XX,+16[1] or 42,X,-X,+mar[1]. In cell cultures, $p53^{+/+}$ cells derived from a recipient blastocyst were eliminated, resulting in occupation by $p53^{C/C1}$ cells with AmCyan1 expression (Fig. 6c).

These findings demonstrate that $p53^{-/-}$ ESCs exhibit several features of abnormalities, such as blockage of differentiation, induction of chromosomal instability, and escape from apoptosis, which are facilitated when the cells differentiate. Thus, p53 is indispensable for embryonic development in the mutant chimeric models (Fig. 1f) but dispensable in the homozygous models due to bypassing an ESC state (Fig. 1e).

Discussion

Here, two distinct strategies were used to generate *p53* KO rats: conventionally generated homozygous KO and ESC-based mutant chimeras. In the homozyogous KO rats, NTDs such as exencephaly and spina bifida were observed. This is the first NTD model created in genetically modified rats. Previously, a 50% reduction in the number of females relative to males at weaning was observed in *p53* homozygous KO mice[17]. In contrast, in the present study, a 96% reduction in the number of *p53* homozygous KO female rats surviving to weaning relative to homozygous KO males was observed (Table 1). In rats, exencephaly occurred in a large fraction of the homozygous KO females (55%; Table 1), whereas only 8–16% of homozygous KO female mouse embryos exhibited exencephaly[17,18]. The survival ratio and spina bifida phenotype observed in these exencephalic rat embryos suggests that this species exhibits more severe phenotypes than mice. We hypothesize that rats are more sensitive to the stress of DNA damage than mice. Consistent with this observation, rat ESCs are more sensitive to differentiation signals than mouse ESCs, which is one reason why rat ESCs were not established until 2008. Mouse ESCs are very stable compared to other species. In mouse, successful chimera contribution and germline transmission using *p53*-null mouse iPSCs has been reported[24,25]. These results were unexpected, considering the vast amount of data regarding the effects of p53 on cell cycle arrest, apoptosis, and DNA

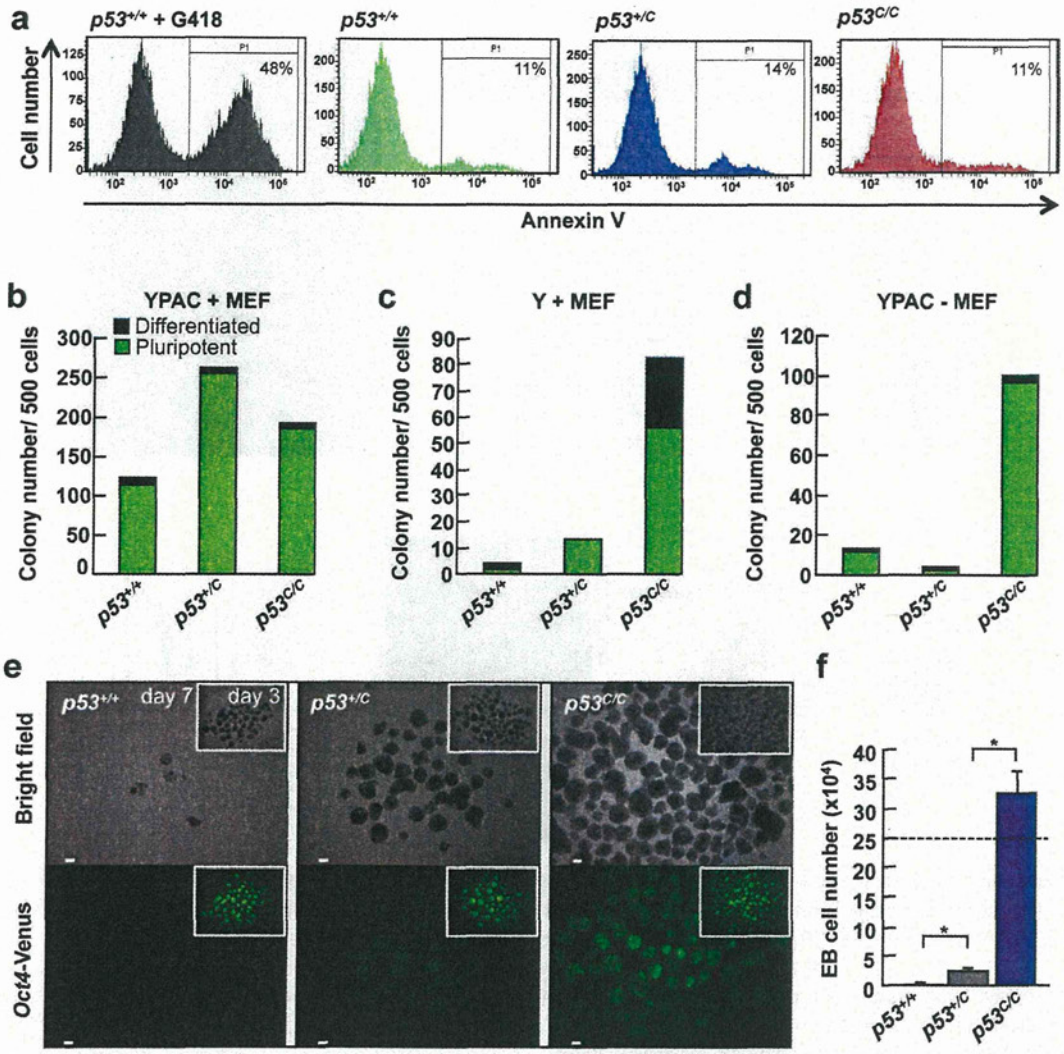

Figure 5 | Colony and EB formation assays under differentiating conditions. (a) Flow cytometry analysis. Annexin V-Cy5 was used to detect apoptotic cells (n=3). (b–d) Colony formation assay. Five hundred cells were cultured under normal conditions (YPAC+MEF; b), differentiation conditions (Y+MEF; c), or apoptosis-inducing conditions (YPAC-MEF; d). A green or black bar indicates pluripotent or differentiated colony number, respectively (n=3 or 4). (e, f) EB formation assay. EBs were formed from 2.5×10^5 cells (f, dotted line). Seven days after incubation without inhibitors, the cell number was counted (f, n=3). Insets (e) indicate EBs at day 3. *, $P < 0.01$. All scale bars = 100 μm.

repair. In contrast, in the present study, mutant chimeras generated with rat ESCs demonstrated a clear phenotype of embryonic lethality, consistent with the data presented here showing the down-regulation of *p53* target genes, inhibition of apoptosis and differentiation, and increase in chromosomal instability in *p53*-null rat ESCs or ESC-derived cells.

The rat is considered to be a better model than the mouse for many complex disorders that are common in humans[36] and is currently the primary animal model in many preclinical tests, especially those related to cardiovascular disease, diabetes, breast cancer, chronic inflammatory diseases, and age-related diseases[20]. Genetically modified rats are valuable platforms for the study of human physiology and disease. For example, in comparison to transgenic mice, transgenic rat models of Huntington disease not only present a more typical adult patient pathology but are also more suitable for *in vivo* metabolic and structural imaging[20,37]. In addition, *Apc* knockout mice develop tumors primarily in the small intestine, whereas both humans and rats develop colon cancer as a result of the *Apc* mutation[38]. These observations support the inconsistent phenotype of *p53* mutant chimeras between rats and mice, as shown in the present work, and suggest the importance of generating genetically modified rats to find novel gene functions.

In this study, the differences in the phenotypes of the *p53* homozygous and mutant chimeric rat models were striking. Secondary mutations are accumulated in the mutant ESCs under *in vitro* culture conditions and in the differentiating cells during embryogenesis (Fig. 6). These aberrant cells are resistant to apoptosis due to *p53* deficiency, which might lead to lethality of the mutant chimeras. These observations reflect the fact that a major p53 function is to be the "guardian of the genome". Thus, the mutant chimeric strategy may prove useful in identifying authentic and/or novel gene functions. Finally, the present study demonstrated that mutant chimeric models can be generated within one month, circumventing both the risks associated with producing successful germline transmission as well as the time frame required for breeding both chimeras and heterozygous animals. In the mutant chimeric method, double or triple gene knockouts can be generated in a few months. These new combination strategies using embryonic stem cells, the mutant

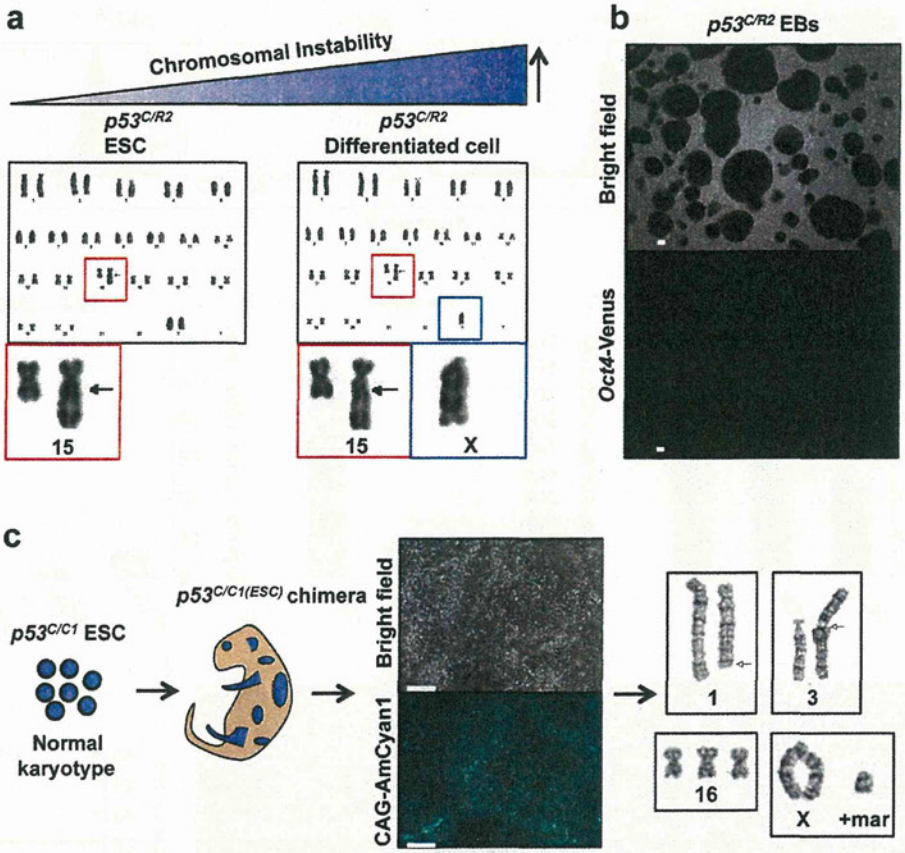

Figure 6 | Chromosomal instability in *p53*-null cells. (a) Cytogenetic analysis by G-band staining in $p53^{C/R2}$ ESCs and EB-derived differentiated $p53^{C/R2}$ cells. Abnormal chromosomes were indicated by red and blue squares. (b) Differentiated $p53^{C/R2}$ EBs lacking Venus fluorescence. (c) Aberrant chromosomes were observed in cells derived from a $p53^{C/C1(ESC)}$ chimera at E14.0.

chimeric method, and rats instead of mice will provide great insight into the novel functions of a large number of genes. The first example, shown here by deleting the *p53* gene, provided new, substantial evidence demonstrating that p53 functions not only as the "guardian of the genome", but also as the "guardian of the embryogenesis".

Methods

Media, feeder cells, animals, and primers. The YPAC medium was prepared by the addition of the following inhibitors: 10 μM Y-27632 (WAKO), 1 μM PD0325901 (Axon Medchem), 0.5 μM A-83-01 (TOCRIS), and 3 μM CHIR99021 (Axon Medchem) to a basic medium. The basic medium was composed of DMEM (including 110 mg/L sodium pyruvate and 200 mM GlutaMAX, GIBCO), 20% FBS (ES Cell Qualified Fetal Bovine Serum, Lot No. 1204059, GIBCO), 0.1 mM 2-mercaptoethanol (SIGMA), 1% nonessential amino acid stock (GIBCO), and 1× antibiotic antimycotic (GIBCO). Mitomycin C-treated MEFs resistant to neomycin (Millipore) were used as feeders and maintained in 10% FBS DMEM (Lot No. SFB30-1502, EQUITECH-BIO, INC.) with 1× antibiotic antimycotic. Animal experiments were performed in compliance with the guidelines of the Institute for Laboratory Animal Research, National Cancer Center Research Institute. These studies were approved by National Cancer Center Research Institute. All primer sequences are listed in Supplementary Table 3.

Generation of *Oct4*-Venus Tg rats and ESCs. *Oct4*-Venus Tg rats of the Wistar strain were generated via germline transmission of an *Oct4*-Venus ESC clone in the same manner described previously[12]. The *Oct4*-Venus ESC line derived from the Long-Evans Agouti (LEA) strain was generated in an earlier study[12].

Establishment of rat ES cells from blastocysts. Rat blastocysts were gently flushed out from the uteri of E4.5 or E5.0 pregnant rats with a basic ES medium. After removal of the zona with acid Tyrode's solution (Ark Resource Co., Ltd.), whole blastocysts were plated onto 6-well plates and cultured on MEFs in basic ES medium with or without YPAC. After approximately 7 days, the blastocyst outgrowths were cut into pieces and replated under the same YPAC conditions. Emerging ESC colonies were then dissociated with Accutase (Innovative Cell Technologies, Inc.) and expanded. Domed and floated ESC colonies were detached from MEFs by pipetting, followed by routinely passaging every 3–4 days under MEF-YPAC conditions.

ZFN constructs and targeting plasmids. Custom-designed ZFN plasmids and ZFN-encoding mRNA for the rat *p53* gene were purchased from Sigma-Aldrich. The design, cloning, and validation of the ZFNs were performed by Sigma-Aldrich. The ZFN pair recognizing exon 4 of the *p53* gene was 5′: TTCTCCAGTCTTCCTCCAG, 3′: ATTCTGGTAAGGAGCCGG. The targeting donor was composed of the CAG-AmCyan1-IRES-Neo-pA or CAG-tdTomato-IRES-Neo-pA cassette with short homology 5′ (736 bp) and 3′ (711 bp) arms. These homology arms were amplified from rat genomic DNA using the KOD Ver.2 DNA polymerase PCR system (Toyobo). The sequences of these primers are listed in Supplementary Table S3. Both arms were set at several base pairs from a ZFN-induced cleavage site.

Introduction of the targeting vector and ZFNs into LEA rat ESCs and generation of *p53* heterozygous rats. To disrupt exon 4 of the *p53* gene, 5 μg of ZFN-encoding mRNAs and 10 μg of a targeting plasmid (5′arm-CAG-AmCyan1-IRES-Neo-pA-3′arm cassette) were co-transfected into 6.5×10^5 of *Oct4*-Venus ESCs derived from a LEA female strain at passage 5 with a Mouse ESC Nucleofector Kit (Amaxa Inc.). The cells were plated on MEFs in YPAC medium with 2% Matrigel (BD Biosciences) to keep the ESC colonies adhered to the MEFs. One day after nucleofection, geneticin was added to the YPAC medium at 0.2 μg/ml. Eleven days after nucleofection, geneticin-resistant colonies were selected using handmade capillaries and expanded. Picking and expanding seven colonies provided four (57%) heterozygous ($p53^{+/C}$) clones and two (29%) homozygous clones harboring both knock-in and frame shift mutation alleles ($p53^{C/Z}$) (Supplementary Fig. S1a). The ZFN-induced frame shift mutation was identified by band shift in PCR analysis (Supplementary Fig. S1a, No. 6 clone, asterisk) and sequence analysis (Supplementary Fig. S1c) or using a SURVEYOR Mutation Detection Kit (Supplementary Fig. S1b, No. 8 clone). A $p53^{+/C}$ ESC clone was used for microinjection, resulting in the generation of $p53^{+/C}$ rats through chimeric germline transmission.

Introduction of the targeting vector and ZFNs into Wistar rat ESCs. For nucleofection, 10 μg of a targeting plasmid (5′arm-CAG-AmCyan1-IRES-Neo-pA-3′arm